Technical Design Report

Washington State University-Everett with Everett Community College

MAY 23RD, 2021

Team Members

Alyssa Gorrell WSU-Everett Team Lead	Sarah Hastings WSU-Everett Aerodynamics	Kaitlin Jones WSU-Everett Project Development	Melody Ripsom WSU-Everett Digital Content Creator
Isaiah Funston WSU-Everett Team Lead	Jessica Kupcake WSU-Everett Digital Content Creator	Sam Ayars EvCC Electrical Design	Elena Bahr WSU-Everett Social Media Manager
Kaleb Willis WSU-Everett Rotor Design	Minhkennedy Pham WSU-Everett Rotor Design	James Garfield EvCC Electrical Design	Kayla Haus WSU-Everett Outreach Coordinator
Tahier Seid WSU-Everett Rotor Design	Eliza Goodwin WSU-Everett Project Development	Ben Austin EvCC Communications	Elijah Lovold EvCC Electrical Design
Nathan Blackwell WSU-Everett Content Creation and Digital Outreach	Jackson Wagner WSU-Everett Control System Design		

Advisors

Dr. Gordon Taub WSU-Everett Principle Investigator	Joe Graber EvCC Co-PI	Mike Patching EvCC Co-PI

Executive Summary

The material presented in the following document was conducted through participation in the Department of Energy's 2021 Collegiate Wind Competition (CWC). The Washington State University-Everett and Everett Community College Wind Energy Team, continuing their work from last year, to design and build a cycloturbine, a type of vertical-axis wind turbine notable for its ability to produce more power than the traditionally inefficient vertical-axis turbines. Traditional vertical-axis turbines are known for their inability to self-start and their low efficiency. Cycloturbines add a mechanism to this type of turbine to move the blades in a more efficient way, eliminating both of these problems. Additionally, cycloturbines are an area of active research, which interested the team. Choosing to design a cycloturbine let us work on a largely unexplored area of turbine design.

Cycloturbines are usually built as mid-sized turbines, so the Everett Wind Energy Team was challenged with building one small enough for the CWC. One downside of cycloturbines is that they have more moving parts than a traditional vertical axis turbine, which was difficult to make efficiently at this scale. The team has done their best to design a mechanism which works at this scale, taking great steps to simplify the design from last year and reduce the part count.

Vertical axis turbines inherently have more complicated aerodynamics than traditional horizontal axis turbines, and the aerodynamics of cycloturbines are increasingly complex due to the additional movements of the blades. Because of this, there is no readily available cycloturbine analysis tool, leading the team to develop their own analysis codes.

For the electrical and control system, the team focused on optimizing power production under wind speed conditions up to 11 $\frac{m}{s}$ while utilizing an active yaw control system. A three-phase permanent magnet brushless motor was chosen for a generator, then converted to DC via a three-phase bridge rectifier. While developing the control systems, it was decided to omit measuring wind speed and instead use information about the rotational speed, from a Hall effect sensor built into the generator, as well as current and voltage, reported by a DC Current Monitor, to monitor the system with an Arduino at the center. A variable load of parallel resistors is controlled by the Arduino and allows the system to adjust the torque towards optimal conditions by increasing or decreasing the current.

Traditional vertical-axis wind turbines do not require a yaw system, however, because cycloturbines pitch their blades based on the direction of the wind, a yaw system is needed. An active yaw system monitors the direction of the wind and adjusts the pitching mechanism accordingly. The team originally intended to include a mechanical brake in our design to control the turbine as needed. Studies were done on braking systems, and a prototype was built. However, it was decided to not include the mechanical brake in our final design.

The team was able to construct a full prototype of the turbine despite the COVID-19 lab restrictions, and spent time creating a testing apparatus to mimic the CWC wind tunnel conditions. The turbine ultimately suffered from mechanical issues preventing the full assembly from working, but many parts of the design will lend themselves to next year's competition. This year's competition has strengthened the team's understanding of wind energy concepts. Choosing to focus our efforts on a cycloturbine design allowed us to participate in active research and immerse ourselves in a growing field. Extensive progress has been made and we look forward to continuing our progress next year.

Table of Contents

I. Introduction

Traditional horizontal axis wind turbines have been researched and developed for decades. They are functional, well understood, proven designs. Vertical axis wind turbines, by contrast, are not as well understood and generally produce less power. Both turbine types have their advantages and disadvantages; horizontal axis wind turbines produce high power and are easily scalable, while vertical axis wind turbines are easier to manufacture and maintain. Our team picked a vertical axis design because vertical axis wind turbines are not as well understood and have a lot of room for research. The goal of this competition is to learn, and we felt we could do that best with a vertical axis wind turbine.

The aerodynamics of horizontal axis wind turbines (HAWTs) are relatively straightforward. There are software packages available, such as QBlade, that can rapidly analyze the aerodynamics of a HAWT. HAWT blades undergo steady forces, that is, each point on a HAWT blade experiences a uniform aerodynamic force regardless of its angular position. Vertical axis wind turbines (VAWTs) have significantly more challenging aerodynamics. VAWT blades are subject to cyclically varying aerodynamic forces. A blade producing useful lift on one side of the turbine may be completely stalled on the other side of the turbine. These cyclically varying forces are largely responsible for the poor performance of traditional VAWTs. Most VAWTs have fixed-pitch blades. Their blades are set at some constant angle with respect to the turbine. When a fixed-pitch VAWT spins, there is nothing to prevent the blades from stalling at some locations, which impairs their performance. Our design is a variable-pitch VAWT, also called a cycloturbine. Cycloturbine blades pitch as the turbine spins to respond to the varying aerodynamic forces, which greatly increases their performance. The blades can be pitched to maximize their performance and prevent stall. **Figure 1** shows an example of the cyclic blade motions of a cycloturbine.

Cycloturbines have been shown to produce much more power than fixed-pitch VAWTs [2], even being competitive with HAWTs, which is why our team originally chose to design one. Vertical axis wind turbines offer several advantages over traditional horizontal axis wind turbines (HAWTs). HAWTs have their machinery high up in a nacelle, which is difficult and hazardous to maintain, while VAWTs have all their machinery easily accessible on the ground. HAWTs have varying wind velocities along their blades, so their blades are twisted and tapered to account for this, which improves their efficiency, but makes them difficult to manufacture. VAWT blades, by contrast, can have constant profiles which make them easier to construct. Additionally, VAWTs have their center of gravity closer to the ground, making them more suitable for offshore applications than HAWTs, which are difficult to keep upright when offshore.

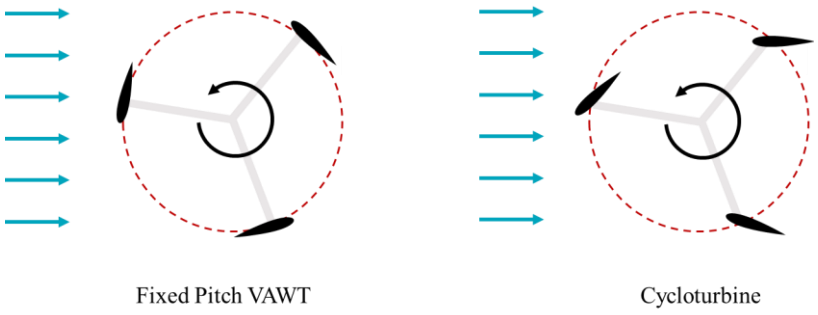

Figure 1: *Top view of fixed pitch VAWT vs cycloturbine*

Our cycloturbine for the 2021 Collegiate Wind Competition (CWC) is a continuation of our design from last year. Last year, our design was very complex, and a lot of our work this year went into simplifying that design to a producible model. An overview of our design and design decisions can be found in **Section II**. The details of our aerodynamic analysis can be found in **Section III**, while the rest of our mechanical design can be found in **Section IV**. Our electrical and control system design are described in **Section A**. The experimental verification of our prototype is in **Section VI**, and our conclusion is in **Section VII**.

II. Design Objectives and Components

The objective of our turbine design team was to create a turbine that performed well in the CWC test environment. The turbine had to fit within the bounding box shown in **Figure 2**. The bounding box is a 45 cm cube mounted on a 15 cm diameter cylinder which extends 37.5 cm downwards from the bottom of the cube. The turbine blades needed to be completely enclosed in the cube.

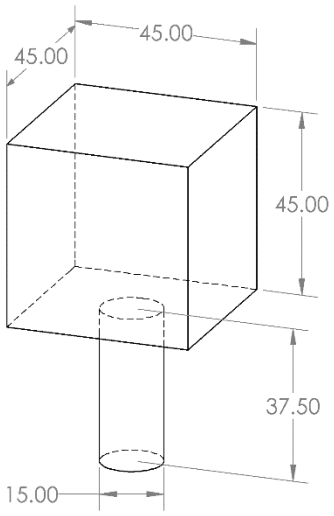

Figure 2: *Turbine bounding box*

The turbine was supposed to start at the lowest wind speed possible, then produce power of varying levels until wind speeds of 11 m/s, after which it would produce constant power. All turbine components were designed to withstand wind speeds of 22 m/s.

The electrical system needed to work with an out of box motor to be used as a generator. The motor produced AC power which needed to be converted to usable DC power. A system to adjust resistance on the circuit to maintain optimal power output during the variable conditions, as well as apply resistive braking to help prevent runaway speed from being reached also needed to be designed. Finally, a control system needed to be designed to adjust yaw based on wind direction and maintain maximum torque generated from the wind. The cycloturbine requires a yaw system because its pitching scheme is optimized for a certain wind direction, unlike traditional VAWTs which don't need them (**Figure 1**).

We started with our turbine design from last year but tried to simplify it as much as possible for this year's design. Like last year, we used a cam system to pitch our turbine blades as opposed to an active pitching mechanism which would require actuators (**Figure 3**). As **Section III** will explain in more detail, a cycloturbine's pitching scheme can be optimized around a certain tip speed ratio (λ). Tip speed ratio is defined as:

$$\lambda = \frac{\omega r}{V_\infty} \tag{1}$$

where ω is the turbine's rotational speed, r is the turbine's radius, and V_∞ is the velocity of the freestream wind. Last year, we tried to design multiple cams, and a mechanism that would shift between them so that the turbine would always have an optimal cam shape, but this year, that was decided to be too complicated, so we simplified our design to only have a single cam.

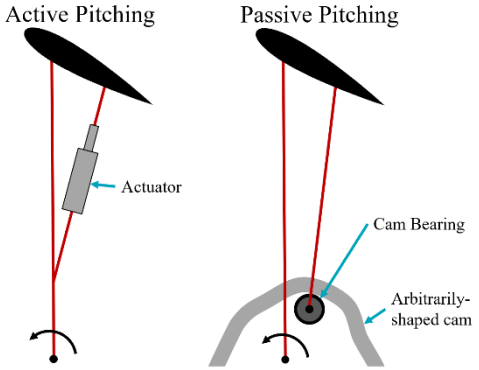

Figure 3: *Active vs passive pitching*

III. Aerodynamic Design

A. Aerodynamic Analysis

Cycloturbines can perform much better than fixed-pitch VAWTs, but they are much more difficult to analyze. Programs like QBlade, which work well for HAWTs, have the capability to analyze only fixed-pitch VAWTs. There is no cycloturbine aerodynamic analysis tool readily available, so it was necessary to write our own aerodynamic codes. Our aerodynamic codes use flux-line theory, a recently developed momentum model developed specifically for cycloturbines.

Flux-line theory was developed by Zach Adams and Jun Chen, two researchers at Purdue University. It is an improvement on the double-multiple streamtube model traditionally used to analyze VAWTs. As a momentum model, it uses actuator disks. Actuator disk theory models the complex blade-fluid interactions

by modeling an infinitely thin disk within a streamtube where energy is removed from the stream. This modeling strategy lowers the computational cost of the aerodynamic calculations. HAWTs can be modeled

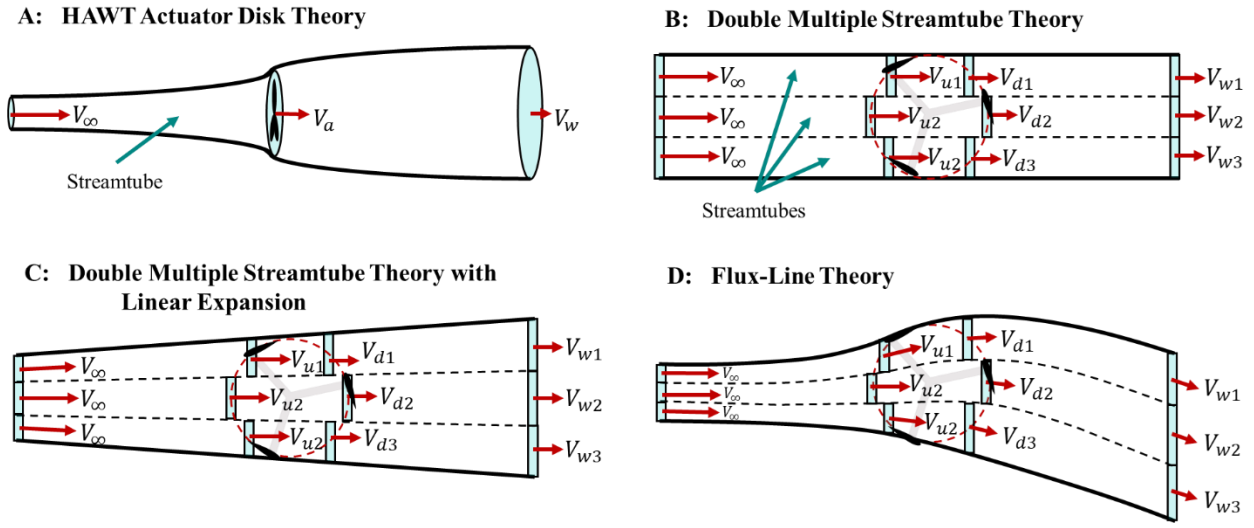

Figure 4: *Streamtube models*

with this theory using a single streamtube and actuator disk, since the entire turbine spins in a plane perpendicular to the wind direction. However, VAWTs are not so simple. All air that passes through the turbine interacts with the blades twice, and the turbine does not spin in a plane, complicating the actuator disk setup.

Figure 4 shows several actuator disk setups. **Figure 4A** shows the setup for a traditional HAWT. The entirety of the air that is processed by the turbine is enclosed in a single streamtube, which has a single actuator disk at the rotor. The streamtube expands as the air slows down. This approach works well for HAWTs, but poorly for VAWTs. **Figure 4B** shows the double multiple streamtube model, which is more tailored to VAWTs. Rather than a single streamtube, the double multiple streamtube model divides the airflow into many smaller streamtubes, each of which has two actuator disks: one for upstream and one for downstream. This better reflects the geometry of a VAWT, but this theory does not allow for streamtube expansion. Blade-element momentum models like these are very sensitive to the airfoils' angle of attack, so it is important to model the path of the oncoming air as accurately as possible, and the assumption that

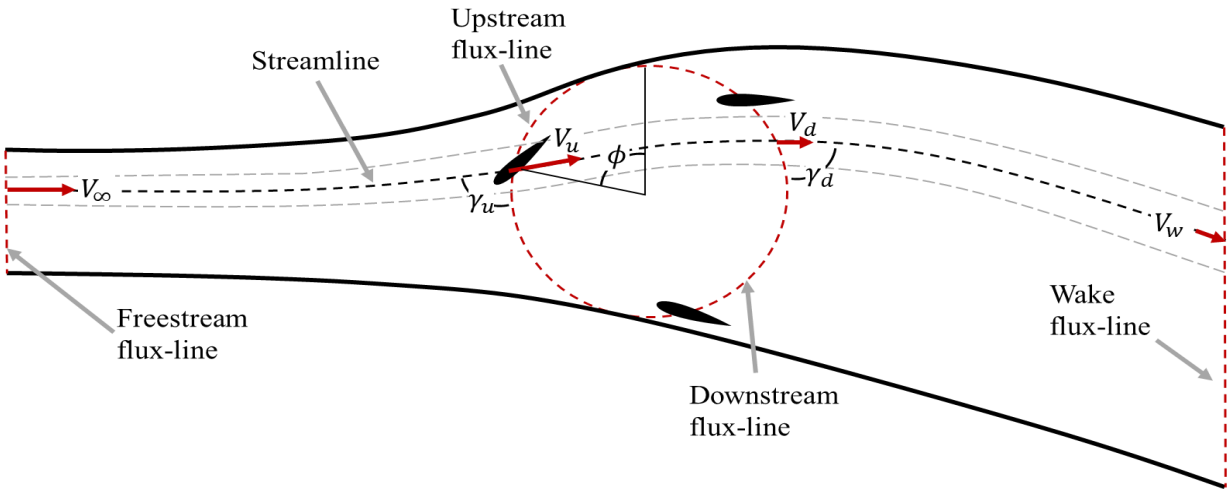

Figure 5: *Flux-line theory*

all the wind travels through the turbine without expansion or deflection is incorrect. **Figure 4C** shows a model which allows flow expansion within the double multiple streamtube model but assumes that the flow expansion is linear. There is no reason to make the flow expansion linear other than to simplify the calculation. **Figure 4D** shows the streamtube distribution of flux-line theory, which allows the streamtubes to both bend and expand. Flux-line theory has been shown to give more accurate results than the other streamtube models by giving the streamtubes this additional flexibility.

The flux-line model is shown in more detail in **Figure 5**. Each streamtube is analyzed at four points, or *flux-lines*, which is where the theory gets its name. Each streamtube has its properties calculated in the freestream flow, at the upstream and downstream flux-lines (which trace the paths of the blades), and at the wake flux-line. At the upstream and downstream flux-lines, the angle γ dictates how much the streamtube bends. The length of the flux-lines are not fixed, which allows for flow expansion. The downstream flux-line can be longer than the upstream one, as the flow decelerates and expands.

Flux-line theory has two variations: a blade-element model and pure momentum theory. The blade-element model is an iterative method used for performance prediction. It uses blade-element momentum theory. It takes inputs such as the airfoil profile, pitching scheme, tip-speed-ratio to calculate how much momentum is imparted to the turbine blades based on a guessed wind velocity. It uses this information to balance the momentum within each streamtube and reevaluate the streamtube velocities at each flux-line. It then repeats this process until it converges upon a solution where momentum transferred to the blades matches the momentum taken from the streamtube. When convergence is reached, the turbine power is calculated from the forces that the model has determined are applied to the blades.

The blade-element model is useful for the performance prediction of a cycloturbine if the blade pitching scheme is known, but it is computationally expensive, and would be cumbersome to use to optimize a pitching schedule. For this, the pure momentum model is more helpful. The pure momentum model calculates turbine power from the velocity distributions along each flux-line and determines which velocity distribution would produce the highest power coefficient. It is essentially the reverse of the blade-element model. Instead of calculating velocity distributions for a given pitching function, it optimizes a velocity distribution, then determines what pitching function would produce that distribution.

To design our turbine pitching scheme, we used pure momentum theory to take optimal velocity distributions as predicted by Adams and Chen [1], and predict what blade pitching scheme would be necessary to slow the air down in that way. Pure momentum theory is a somewhat simplified version of the blade-element model. It only considers blade lift; one of its assumptions is that blade drag is negligible. Pure momentum theory has formulas for relating blade lift coefficients to velocity distributions, from that, we calculated what lift coefficient would be required at each position around the turbine to get the velocity distribution suggested by Adams and Chen, and from that we could calculate what blade angle would have that lift coefficient. However, to know the relationship between blade angle and lift, we required an airfoil polar. Airfoil polars are readily available for airfoils in a straight flow, but VAWT blades experience a curved flow, called *curvilinear flow*. This is shown in **Figure 6**.

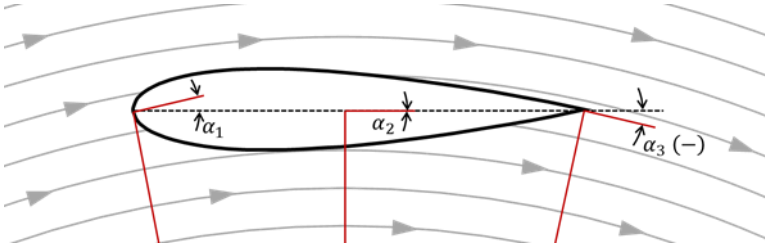

Figure 6: *Curvilinear flow*

Figure 6 shows one of the effects of curvilinear flow, which is that a blade does not experience a uniform angle of attack (α), as blade in a straight (or *rectilinear*) flow would. Commonly available airfoil polars are only valid in rectilinear flow. There are two things that cause these polars to be invalid, one is that airfoils in curvilinear flow have varying local angles of attack along the chord length, and the second thing is that the boundary layer of air around airfoils is susceptible to centrifugal forces, called *centrifugal loading*. Conformal mapping

techniques can be used to account for the variation in angle of attack, but very little research has been done on the effect of centrifugal loading. Additionally, the effects of centrifugal loading vary with rotational speed, so VAWT airfoil polars are dependent upon their tip-speed-ratio. Direct experimental data for a given airfoil and turbine geometry is required to get curvilinear airfoil polars.

We had planned to conduct experiments on airfoils to determine their curvilinear polars, but this was not possible due to the limited lab access allowed during the COVID-19 pandemic. In our codes, we used the experimental airfoil polars generated by Adams and Chen [1] for a NACA 0012. We used a NACA 0018 in our design due to the additional strength it would provide, so the polar is not a *good* match for the behavior of our airfoils, but it was the best we had available.

Using Adams' and Chen's method for translating optimal velocity distributions to blade pitching motions, we obtained the optimal pitching schedules for a tip speed ratio of 1.5. We chose a low tip-speed ratio on purpose, as tests of our mechanical model indicated that the turbine suffered from frictional losses preventing it from reaching higher speeds. The pitching mechanism for our turbine creates a counter-torque which is significant to our turbine at this small scale. Cycloturbines are typically larger than the CWC dictates, and the complex pitching mechanism does not usually present as large of an issue.

B. C_P-λ Curve

While our code for pure-momentum theory is operational, our blade-element codes still need work. Because of this, we cannot yet analytically predict the performance of our turbine. We had planned on testing it experimentally, but this was not possible due to the restrictions on lab hours during COVID-19, and some last-minute mechanical issues that came up, which we will discuss more later. The combination of the lack of real-world testing and the code issues means that we can only estimate our $C_P - \lambda$ curve based on previous work. **Figure 7** shows experimental data from Adams and Chen, along with the prediction from the most successful version of our code. As the figure shows, our code does not yet match the experimental data, which is something that Adams' and Chen's code does very well. We can see that both predict turbine runaway at about $\lambda = 2$, but they have a maximum C_P of about 0.43, while our code only predicts about 0.19. Adams and Chen's experimental data was done on a turbine with the same pitching scheme, and identical proportions to our turbine, but with different airfoils. Both turbines had pitching schemes optimized for $\lambda = 1.5$. We predict that our turbine will produce less power than theirs does due to the added importance of friction at this small scale, but we cannot predict exactly what that is at this time. For the sake of future calculations, we assumed a maximum C_P of 0.3 throughout this paper.

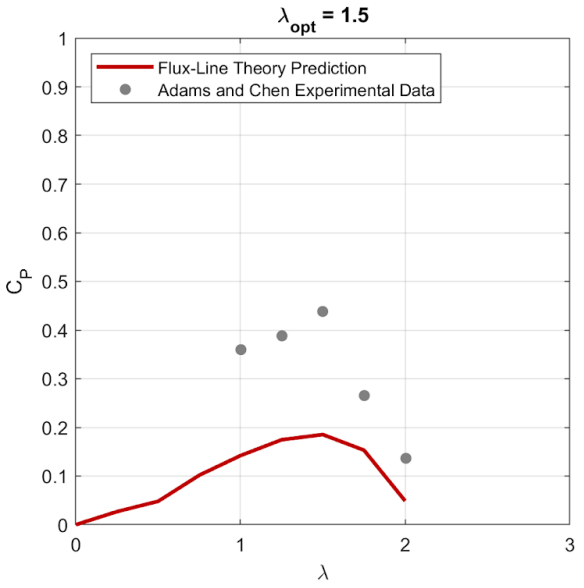

Figure 7: *C_P-λ curve as predicted by our current blade-element code, compared with Adam's and Chen's experimental data for a scaled-up version of our turbine.*

C. Annual Energy Production

Our turbine power curve and annual energy production (AEP) curve is shown in **Figure 8**. The power curve is created using the formula for the power coefficient:

$$P = \frac{1}{2}\rho A V^3 C_P \tag{2}$$

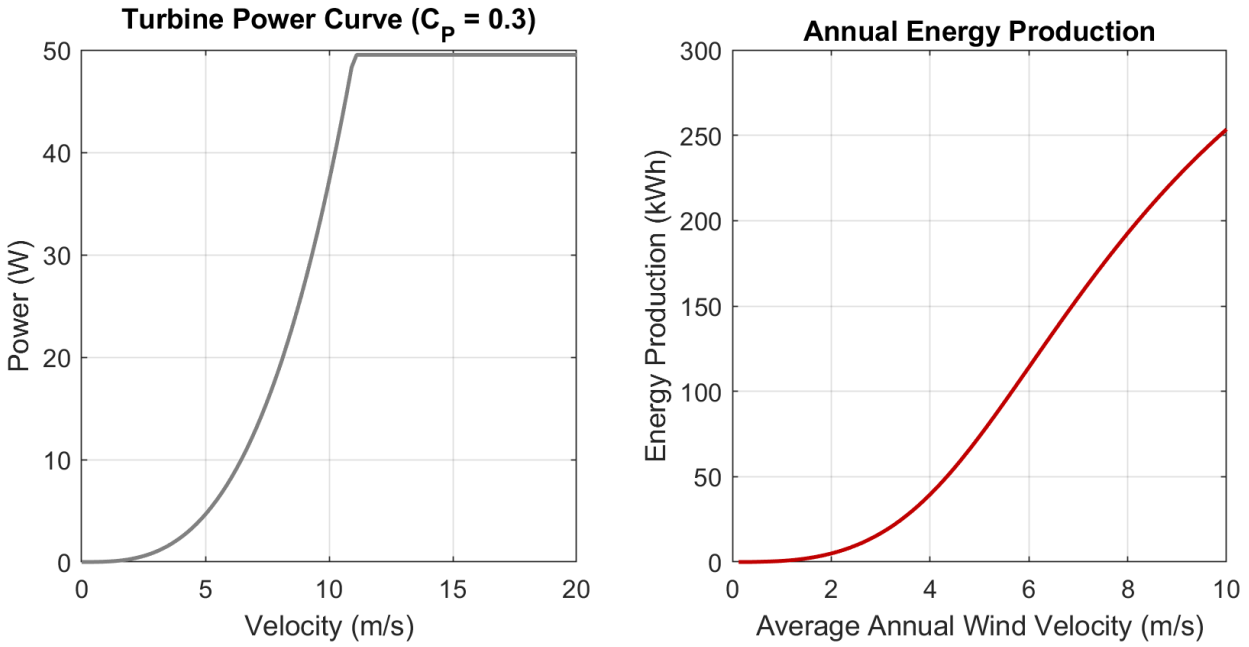

Figure 8: *Turbine power curve and annual energy production (AEP)*

where P is power, ρ is the air density (1.225 $\frac{kg}{m\text{^}3}$, the value around Everett), and A is the projected area of the turbine. This curve is set to a constant after 11 $\frac{m}{s}$, as the CWC dictates. To create our AEP, we first constructed a distribution of wind speeds over the course of a year using a Rayleigh probability density function. (A Weibull function, with shape factor of 2.) A Rayleigh distribution is defined by a single parameter, the scale parameter σ, where σ is related to the mean of the function $\bar{v}$ by

$$\bar{v} = \sigma\sqrt{\frac{\pi}{2}} \tag{3}$$

The mean $\bar{v}$ of the annual wind speed distribution represents the average wind speed over the course of an entire year. For a given scale parameter, we multiply the Rayleigh function by the number of seconds in a year to get a distribution showing the total duration of each wind speed over the course of a year. We then multiply that by our power curve and take the area under the resulting curve to get the total amount of energy produced in a year for the distribution with that scale parameter. We then use Equation (3) to find our average annual wind speed. Doing this for a range of scale factors and plotting a curve of average annual wind speed against total annual energy production, we obtain the AEP curve in **Figure 8**.

IV. Mechanical Design

A. Rotor

The vertical axis wind turbine design employs three equally spaced composite airfoils with their centerlines, each 120 degrees apart. Each airfoil is attached to a cam roller which translates linear motion through the profile of the cam. The cam rollers are connected with unique slide bearings that are built into the lower rotor arm, shown in **Figure 9**. It is connected to the airfoil by a pitch link that is at a set length maintaining an efficient and consistent pitch for each airfoil when rotating. The slide bearing is made of two outer aluminum caps and two plastic bearing liners. The rotor has a slot cut-out where the plastic bearing liners are rubbing on both sides of the rotor. In addition, an aluminum polish was applied on the slots and the sliding surfaces of the rotor to help minimize friction as the airfoils are pitched at various angles throughout the rotation. The arms are then fastened to flanges on the top and bottom of the exposed main shaft.

The main shaft is a combination of precision stainless steel rods. It has two parts: a ¾ inch lower shaft and a ½ inch upper shaft. The upper shaft is concentrically fitted to the lower shaft through a tight tolerance slip fit. There is a bolt that holds the two shafts in place so that the shafts will rotate together. The lower shaft passes through two cylindrical roller bearings, which are integrated into the fixed turbine housing. Cylindrical roller bearings were used because it was able to create a distribution of fiction over a larger surface area which is ideal for a rotating shaft. Moreover, the two bearings make a support couple for the rotor assembly, resisting any moments induced by rotational imbalance and vibration. The lower shaft is rested on the inner race of the upper bearing and consists of a shoulder that locates the shaft vertically. A shaft collar located at the bottom of the lower bearing keeps the shaft from lifting when operating the turbine. The main shaft continues to extend down into the generator housing and engages the planetary gearbox. **Figure 10** shows the configuration of the main shaft assembly.

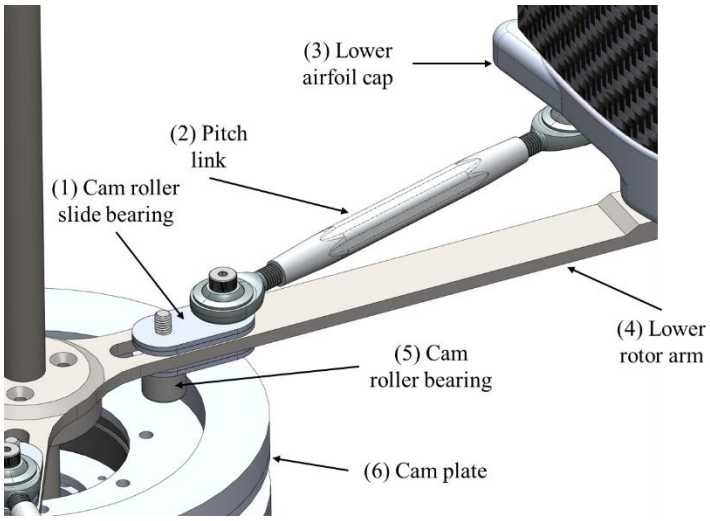

Figure 9: *Close view of pitching mechanism*

B. Column

The column is made of four distinct sections, the yaw system, the shaft bearing section, the generator housing, and the base anemometer section. These sections were designed to separate their functions into sub-components. Although our design this year has the same sub-components as last year's model, this year's design was modified to simplify the mechanical aspects of the yaw system as well as the manufacturability of the parts. The column's outer shell design would require complex CNC machining to make them out of one piece of aluminum. Instead, the shell was designed in multiple parts and then welded together.

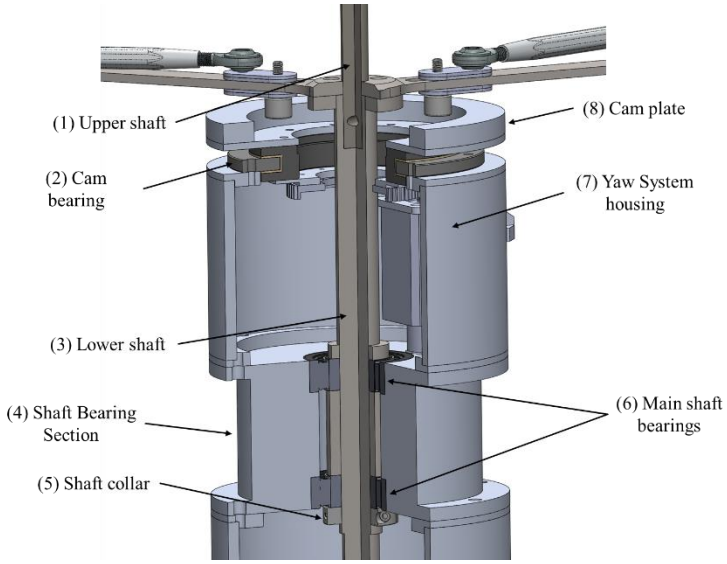

Figure 10: *Main shaft assembly*

C. Yaw system

Unlike a VAWT with a fixed blade pitch, a cycloturbine can vary its blade pitch in order to optimize the performance of the turbine. The optimal blade pitch depends on the wind velocity and current. The cycloturbine needs a yaw system to account for changing wind direction. The turbine is capable of correcting for changes in wind direction through the yaw control of the cam. Rather than rotating the airfoils towards the wind like with a HAWT, our system makes windage adjustments through the yaw control of the pitch scheme cam. The cam platform is fastened to a rotating slewing bearing that allows for a full 360 degrees of rotation. A stepper motor is attached to the bottom side of the slewing bearing through a 5:1 gear ratio in order to turn the pitch cam to account for wind direction. The wind direction is

monitored with a rotary encoder wind vane at the base of the turbine column. An Arduino program is used to take in wind direction change and turn the stepper motor for the pitch cam accordingly.
The optimal pitch scheme is a function of the system's tip speed ratio (TSR). To have an efficient turbine, the system needs to be able to adapt and adjust pitching schemes accordingly. This type of optimization

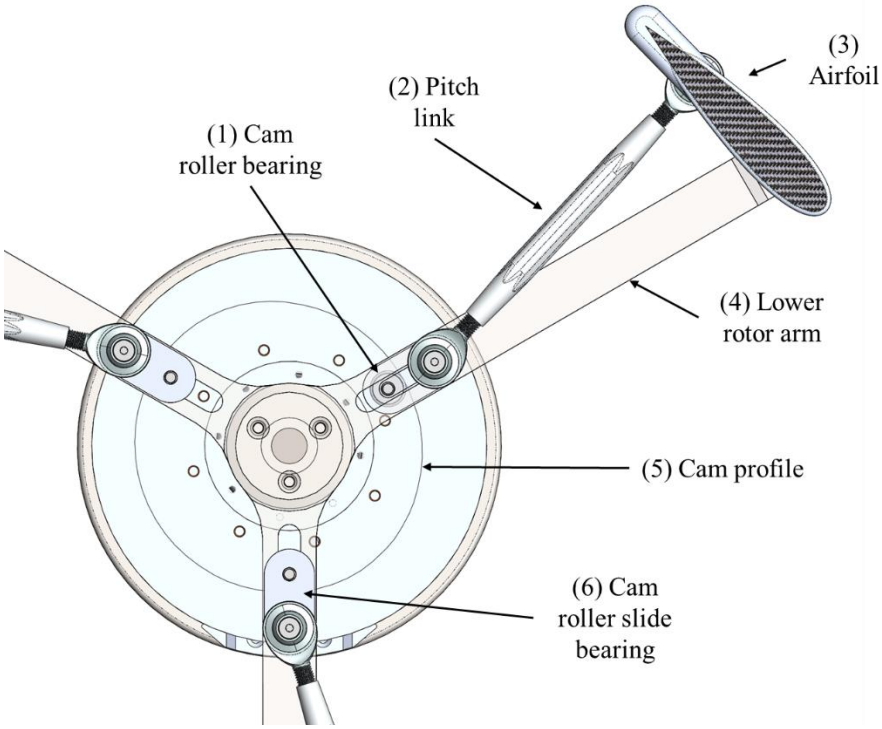

Figure 11: *Top view of pitch mechanism*

would require a different cam pitch profile at different rotor speeds. Although we designed a multiple cam system last year, we decided to switch to a single-stage cam profile to simplify the mechanics of the yaw system. An exploded view of the yaw system is shown in **Figure 11**.

D. Generator

The generator housing sits below the bearing section and houses the generator, planetary gearbox, and brake system (**Figure 12**). The brake system was designed using a brake caliper and rotor sourced from an electric scooter. The caliper originally was operated with a wire cable that applied torque to an arm to squeeze the brake pads against the rotor. However, due to space constraints, the wire cable and arm were removed and replaced with a servo motor attached directly to the caliper to squeeze the brake pad. The servo motor is mounted in the yaw system housing with a shaft passing through the bearing section to reach the brake caliper. This design was

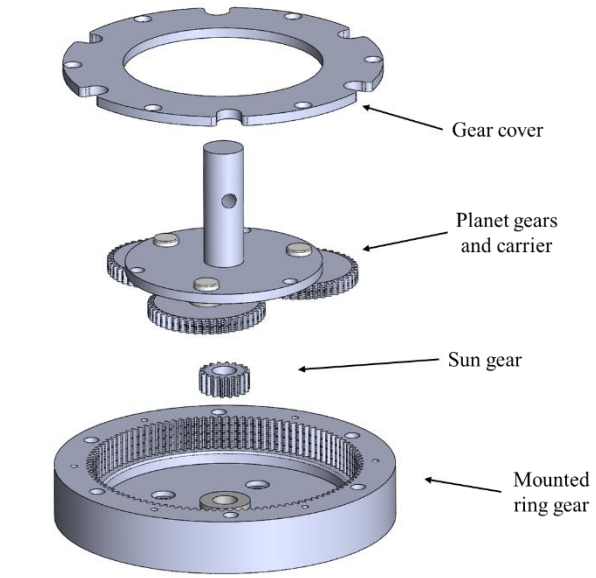

Figure 12: *Gearbox*

chosen to meet the generator housing packaging constraints and minimize manufacturing by using off-the-shelf parts.

A planetary gearbox with a 4:1gear ratio was used to reach the optimal speed for the generator while maintaining an optimal TSR on the rotor side. The planetary gearbox was designed to fit our packaging constraints within the generator housing. Sourcing the correct ring gear for our desired ratio and design was challenging, so we decided to 3D print one using PET-G plastic. This allowed us to incorporate the correct mounting holes directly into the ring gear. The planet gear carrier, which attaches to the main shaft, was made of aluminum and used three brass planet gears. The sun gear connected to the generator is made out of stainless steel.

E. Mechanical Loads

The mechanical loads that our turbine experiences are from vibration, centripetal force, and wind force. Vibrational forces on the system depend on the mass symmetry and balance of the rotor. Static and dynamic techniques can be used to balance the rotating assembly. All rotor components of the assembly will be weighed to ensure mass similarity. A static balance will be done to determine the location of any imbalanced weight once the rotor assembly is complete. The goal is to have the weight of all components distributed equally about the center of rotation. A dynamic balance test can also be performed while the turbine is in rotation using a dynamic balance measuring device.

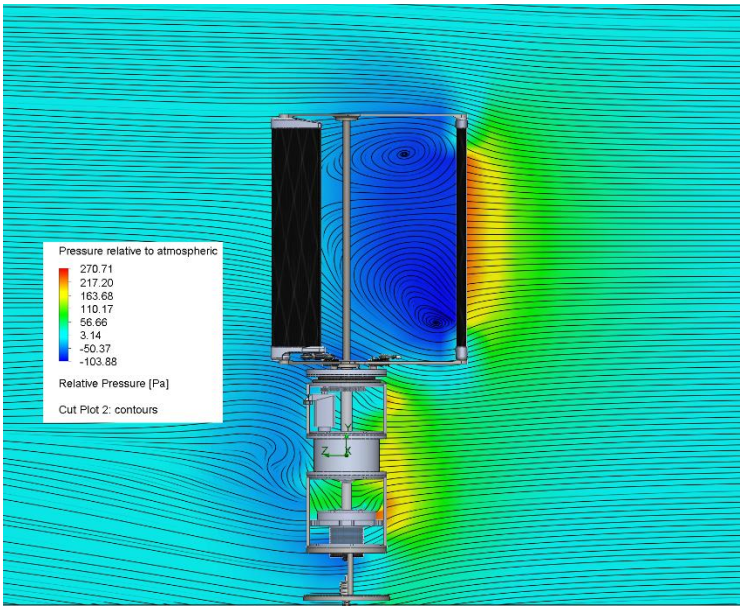

Figure 13: *Flow simulation*

First, we completed a flow simulation (**Figure 13**) with the rotor fixed at a position of max drag force, which is perpendicular to the wind at 22m/s. From this flow simulation, we were able to transfer fluid pressure to FEA analysis to determine the loads at max wind speeds and max drag. As you can see in figure X where the max combined loading was about 35N.

In our next study, we were able to take the fluid force from the wind and exported it into a static FEA study. Where we found that our turbine will hold up to that load since all areas show a Factor of Safety (FOS) of 10. As shown in **Figure 14**. Then in the next study we included the wind load as well as the max RPM of 1400, in addition to where we took into consideration the max lateral and centrifugal loads. Since the turbine would not experience both of these loads at the same time since the wind lid will be significantly less when the turbine is spinning.

The airfoils are to be built with a carbon fiber shell and a skeletal interior structure which cannot be analyzed accurately using SolidWorks simulation features, as the system is missing information on the deformation properties. For the sake of analysis, these airfoils were modeled as a rigid body. We were also able to create custom material for PLA material to include the blades in our analysis. This FEA was done to analyze the rotor arms, airfoil caps, and main shaft of the rotor assembly.

In this FEA study, we simplified the model by treating purchased components as rigid and replacing the links with component connections. In **Figure 15** the factor of safety is shown to be above 2 except for a few stress concentrations that were created due to the simplification made.

In order to run simulations for this model we removed all the shelf components and replaced them with component connections. The sliding pitch links were replaced with a rigid link for the FEA analysis. This rigid link connects at a point instead of sliding in a slot. We are confident that the stress seen at this slot will be much less with the actual pitch link. The location of these connections in question is shown in **Figure 16**.

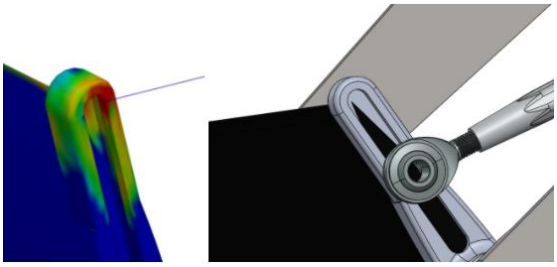

Figure 16: *Close of stress analysis on airfoil caps*

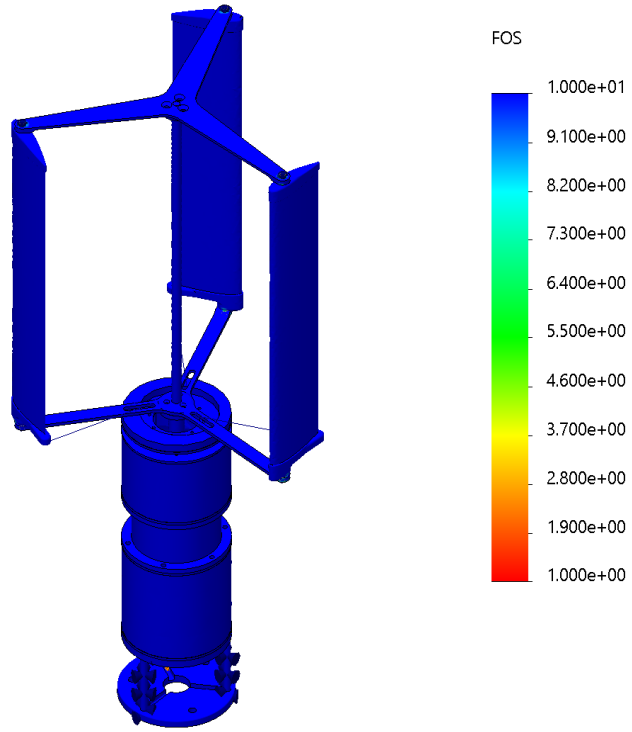

Figure 14: *FOS plot of assembly*

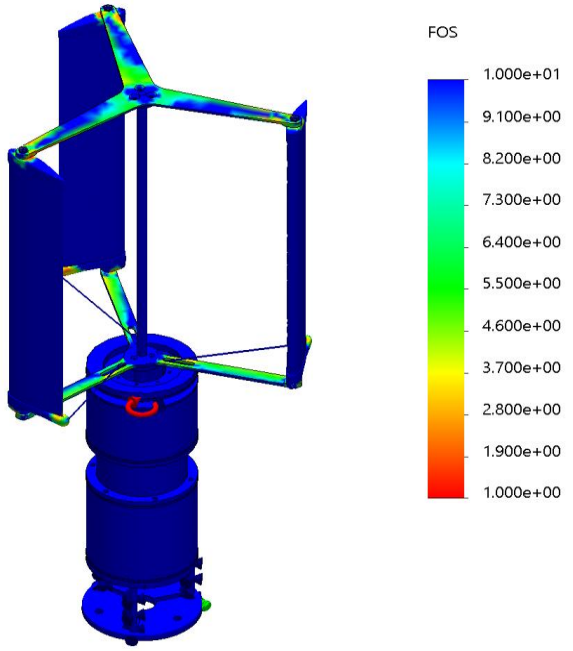

Figure 15: *FOS plot*

V. Electrical Design and Controls

A. Introduction

The electrical systems were designed around a three-phase permanent magnet brushless generator and an Arduino controlled variable load. Current from the generator is converted to DC by a three-phase rectifier and a current sensor sends information to the Arduino. A Hall Effect sensor built into the generator sends rotational information to the Arduino as well. This information is used to adjust our variable load to obtain an optimal torque. Our cycloturbine pitches the blades based on each blade's orientation to the wind as the turbine spins, necessitating a yaw system. The pitching scheme of the blades is controlled by rotating the cam, done based on input from an encoder connected to a small fin for reading the wind direction. Originally a mechanical brake was to be incorporated into the design to help maintain safe rotational speeds when above 11m/s or to provide safety stops when necessary. However, while research and prototyping were done for a mechanical break, it was ultimately not included in the final design due to limited lab time caused by COVID-19. An overview of the electrical and control system can be seen in **Figure 17**.

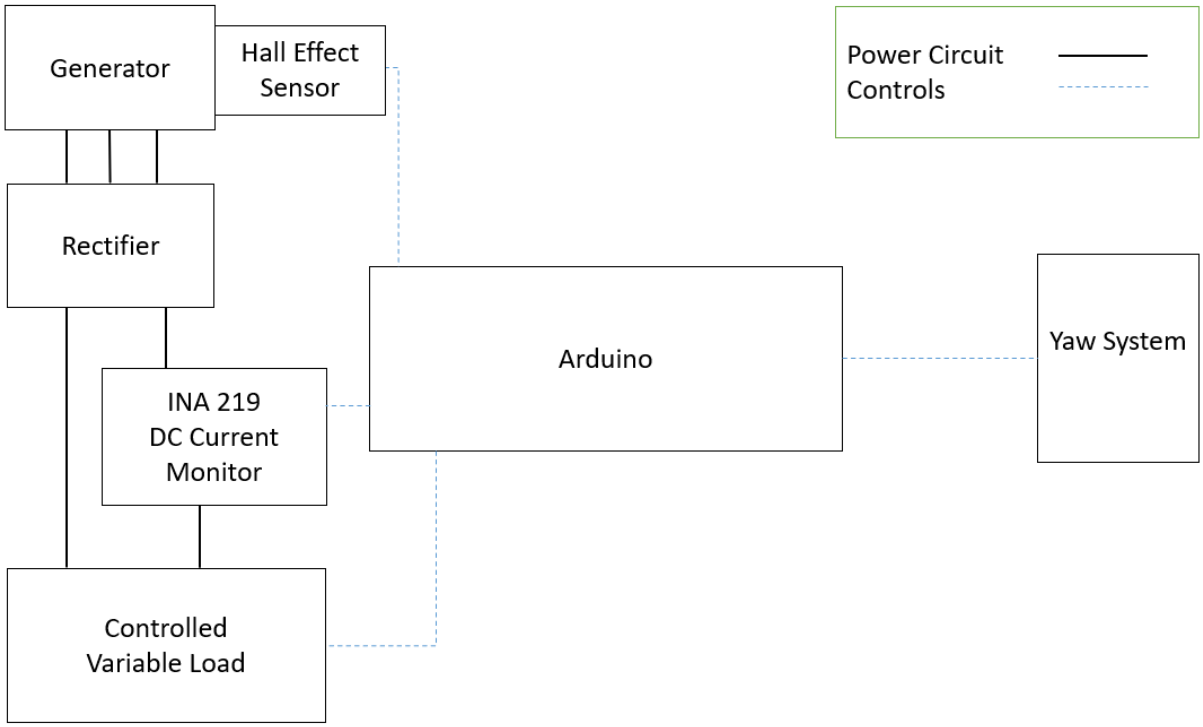

Figure 17: *A simple circuit diagram of the turbine control system, showing how the power and control systems interact. Note that due to time constraints, the yaw system was controlled by a dedicated Arduino Uno rather than integrated into the main Arduino Mega unit.*

B. Generator and Load

With a wide range of motor options available that could be used to convert the rotational energy of the turbine into electrical energy, many options were weighed such as cost, maintenance, efficiency, and size. Ultimately it was determined that a brushless three-phase motor would be the most suitable fit because of the theoretical increase in efficiency due to less internal friction, and longer service life compared to brushed motors.

We chose the Turnigy SK8-6364 Sensored Brushless motor to convert the turbine's mechanical energy into electrical energy. A significant factor in our decision was the motor's 190KV rating, representing the number of revolutions per minute needed per volt of output. We believe this relatively low KV rating will

significantly help with generating usable power at low wind speeds. The Turnigy motor also has a built in Hall Effect sensor, used to measure RPM, which reduces the number of extra components we would have needed to attach to our turbine.

Power generated by the motor is three-phase AC so we are using a rectifier to turn it into DC before sending it to the load. The load we are using is a controlled variable load, allowing extra resistors to be enabled and disabled based on the situation. The load consists of a 10Ω resistor, that is always active, in parallel with five 30Ω resistors that are optionally included in the circuit via MOSFET switches controlled by an Arduino (**Figure 18**). Changing the resistance will inversely influence the amperes of current flowing through the circuit, which in turn will modify the torque experienced by the generator and we use this relationship to maintain optimal power generation conditions. We have placed an INA-219 DC Current Monitor in series between the rectifier and the load to assist with this task.

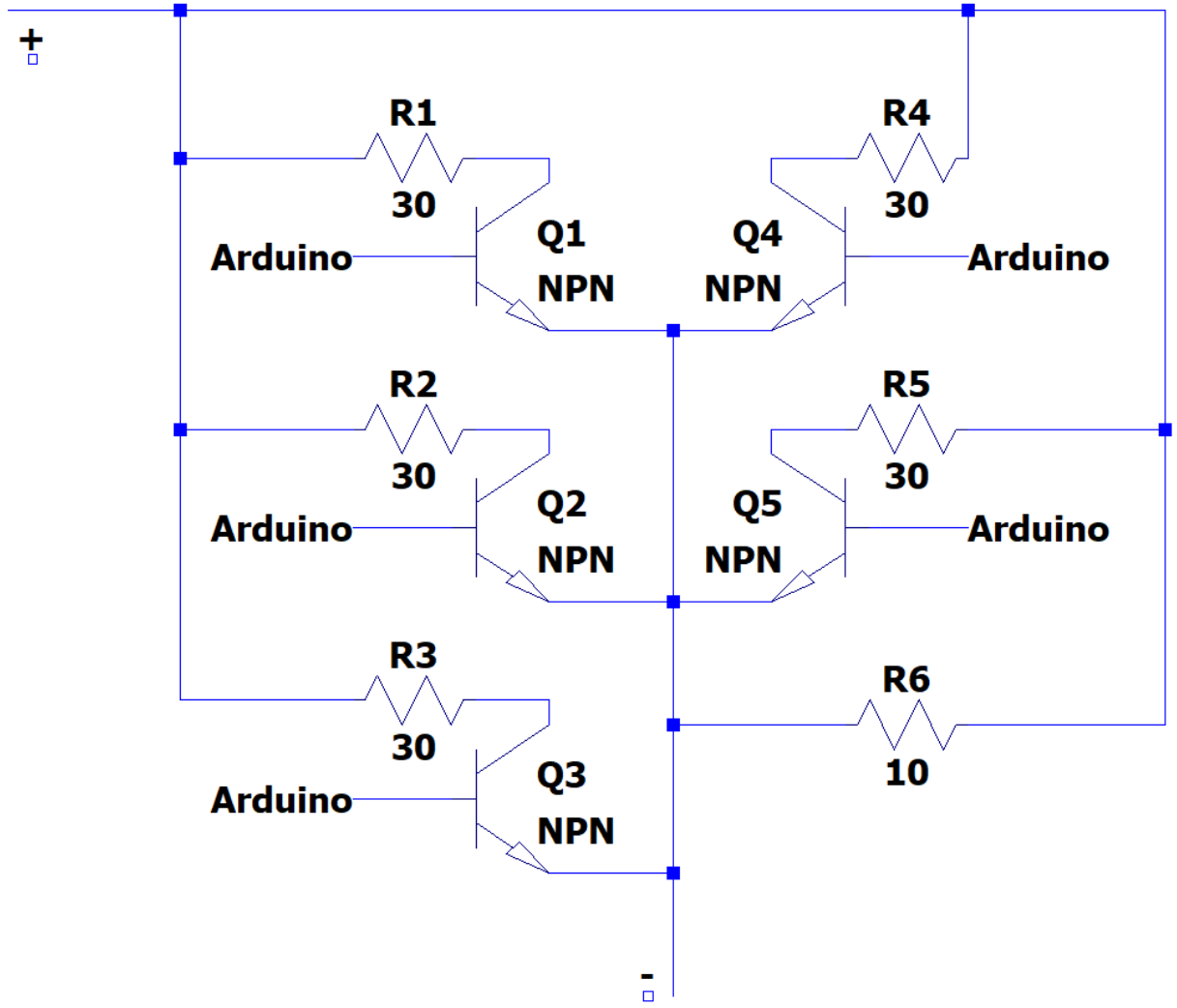

Figure 18: *Controlled variable load schematic. A 10Ω resistor is in parallel with five 30Ω resistors. The 30Ω resistors can be included or excluded from the circuit via NTE2903 MOSFET switches controlled by an Arduino.*

C. Control Theory

Power available in the wind is a function of wind speed (V_∞), air density (ρ), and cross-sectional area (A) is known to be:

$$P_{wind} = \frac{1}{2}\rho A V^3 \tag{4}$$

The torque experienced by the wind turbine, due to the force exerted on it by the wind, is described as

$$T_{mech} = \frac{1}{2}\rho A r V_\infty^2 \tag{5}$$

where r is the radius of the turbine. By introducing a coefficient of performance ($C_P(\lambda)$) we can describe the mechanical power which is extracted as:

$$P_{mech} = \frac{1}{2}\rho A C_P(\lambda) V_\infty^3 \tag{6}$$

The coefficient of performance $C_P(\lambda)$ is a function of the tip-speed ratio (TSR) λ:

$$\lambda = \frac{\omega r}{V_\infty} \tag{7}$$

where r is the radius of the turbine and ω is the rotational speed. Using the λ we can reform (5) into a function of λ and rotational speed:

$$P_{mech} = \frac{\rho A r^3 C_P(\lambda_0)\omega^3}{2\lambda_0^3} \tag{8}$$

Since A, r, $C_P(\lambda_0)$, and λ_0 are all constants, a substitution can made to simplify variables such that:

$$\kappa = \frac{\rho A r^3 C_P(\lambda_0)}{2\lambda_0^3} \tag{9}$$

with κ being determined experimentally. By operating our turbine at the optimal TSR (λ_0), maximum power extraction is achieved. With this in mind, we can define the reference torque T_{ref} for our system as

$$T_{ref} = \frac{\rho A r^3 C_P(\lambda_0)}{2\lambda_0^3}\omega^2 = \kappa\omega^2 \tag{10}$$

And the optimal rotational speed:

$$\omega_{ref}(T) = \sqrt{\frac{2\lambda_0^3}{\rho A r^3 C_P(\lambda_0)} T} = \sqrt{\frac{T}{\kappa}} \tag{11}$$

This allows regulation of the system without wind speed measurement. Using a 1:4 planetary gearbox the goal is to align the torques of the generator T_{gen} and the turbine, based on the current rotational speed ω, such that:

$$\frac{1}{4}T_{gen} = T_{mech} = T_{opt} \tag{12}$$

For a permanent magnet synchronous machine (PMSM), the dynamics of the machine are dominated by the torque constant K_t (in Newton-meters per amp) which was determined by bench testing. The torque on the generator T_{gen} is proportional to the stator current I_s. This current can be adjusted via a controlled variable load and is related to torque by the equation:

$$T_e = K_t I_s \tag{13}$$

With the value of I_s obtained real time from the INA-219 chip in the circuit, and K_t determined experimentally during development, it's possible to calculate the value of T_{gen} at any given point in time. While PMSMs are three-phase devices with resistance and inductance, the rectified EMF E can be approximated by using the generator's K_v rating:

$$E = K_v \omega \tag{14}$$

D. Yaw System

As the competition gives constraints on the turbine design, such as the overall height and width of the turbine, the yaw system was designed to fit within the turbine column that has a maximum diameter of 140mm. The yaw system consists of cam motor housing, the cam bearing, the cam stepper motor, and the cam plate, as shown in **Figure 20.**

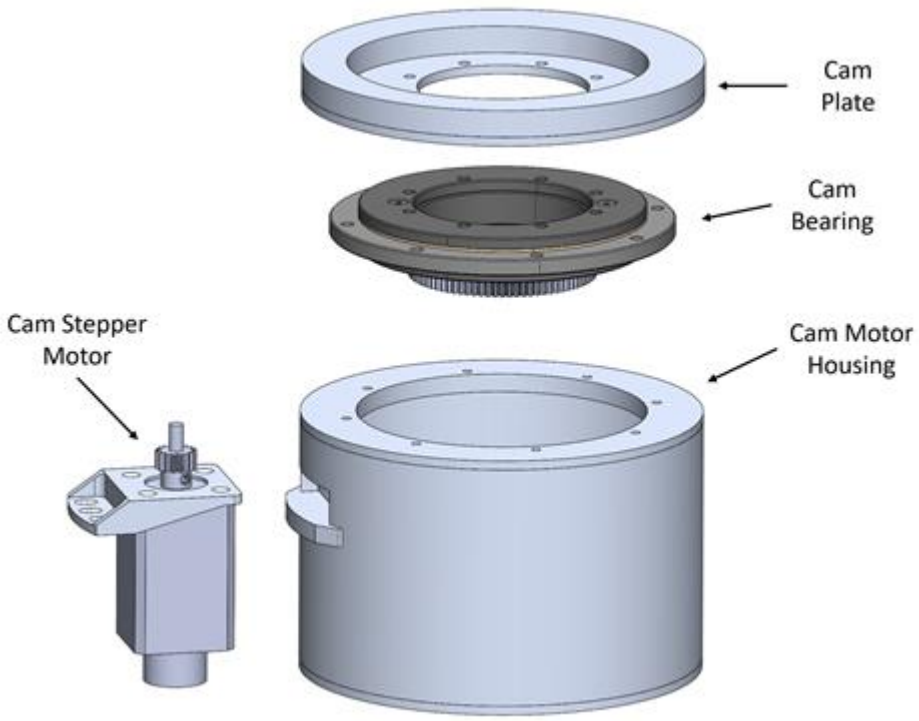

Figure 19: *The exploded view of the yaw control system components*

The cam profile, on the cam plate, is optimized to generate the correct airfoil pitch depending on the direction of the wind. In other words, the cam has a front point that needs to be pointing into the wind to optimize the pitch of the airfoils. The stepper motor was chosen based on the size constraint and the total amount of torque needed to turn the cam plate which is attached to the cam bearing and can spin a full rotation continuously. The cam is used to change the pitch of the airfoils throughout the rotation of the turbine rotor. The stepper motor is also equipped with an incremental rotary encoder to keep track of its rotation. To increase the effective torque of the stepper motor, a 5:1 gear ratio is used between the stepper motor and cam plate. **Figure 19** shows the stepper motor mounted to the cam motor housing.

To know the wind direction, we had to make a wind vane using a rotary encoder with a fin attached for the wind to move. The encoder we used was an absolute analog rotary encoder. The encoder takes in 5 volts and depending on where it is at within the rotation reading outputs a fraction of the input voltage. The

encoder has a scale from 0 to 1023, so in order to make the scale usable, we re-mapped it to 0 to 360 using the map() function. Being an absolute encoder, if the power was disconnected, the encoder still read the same value when reconnected. This is useful as when the turbine is oriented correctly with a certain direction, each direction will read the same encoder value even if the turbine loses power.

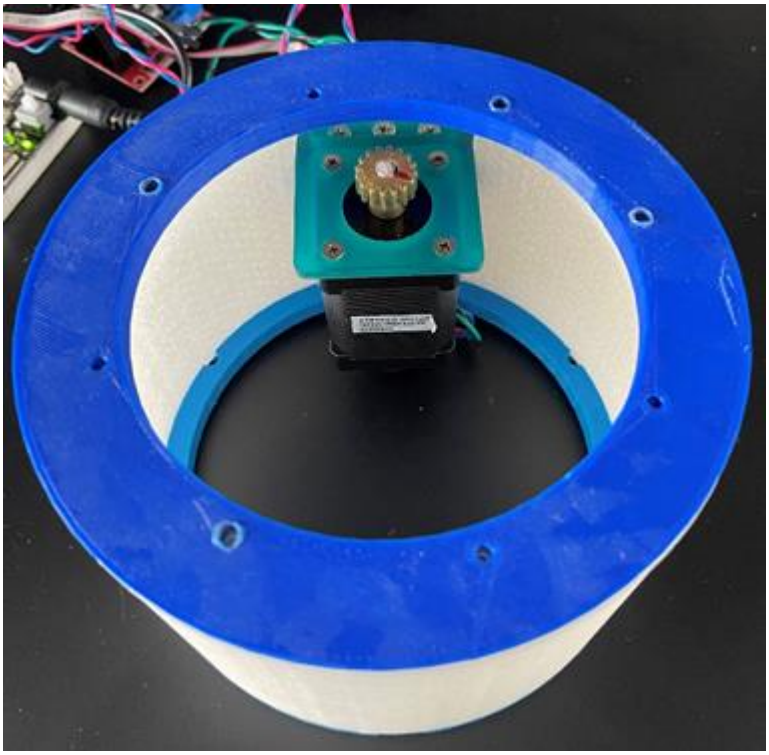

Figure 20: *The cam motor attached to the motor housing.*

Now with the wind vane as our input sensor, we need to control the stepper motor so it can orient the cam plate in the correct direction. To achieve this, we set up a PID controller using the wind vane value as the setpoint and the encoder on the stepper motor as the input, and the output gives step and direction signals to the stepper motor. Since the stepper motor is told how many steps to take, we had to convert the sensor angle of our wind vane to the number of steps to take to achieve the corresponding angle. First, we found out that it takes 200 steps to turn the motor one rotation and we used that to determine that each step is 1.8 degrees. So, we took the input angle from the wind vane and divided it by 1.8 to get the number of steps to turn the motor. Lastly, the motor and cam plate have a 5:1 gear ratio so the result was multiplied by 5 to get the number of steps to move the cam plate to the right output angle.

VI. Experimental Verification

A. Blade Strength Test

The blades on our turbine were 3D printed this year. As finite-element analyses are difficult on 3D-printed plastic parts, we experimentally determined the strength of our blades. We did this by loading a sample airfoil with weights until it broke. The airfoil was supported on both ends by bolts, just like it would be when connected to the turbine (**Figure 21**). To distribute weight across the entire surface of the airfoil, we cut a foam negative of the airfoil (**Figure 22**) which provided a flat surface to stack the weights on (**Figure 23**). We stacked a number of known weights (**Figure 24**) on top of the airfoil until it failed (**Figure 25**). The destroyed airfoil is shown in **Figure 26**. It failed on the joints between the three sections. The airfoil

withstood 60lbs before failure, which is much more than was expected.

Figure 21: *Airfoil setup*

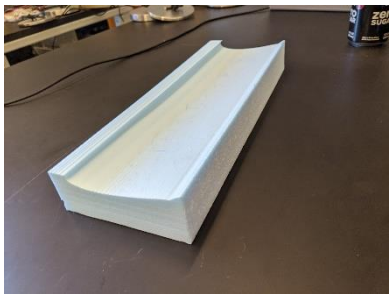

Figure 22: *Foam negative*

Figure 23: *Airfoil ready for testing*

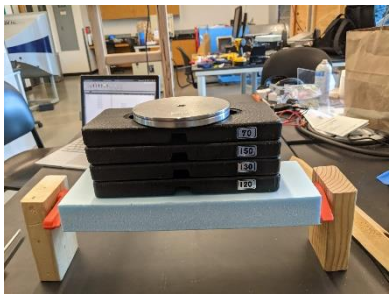

Figure 24: *Loaded airfoil*

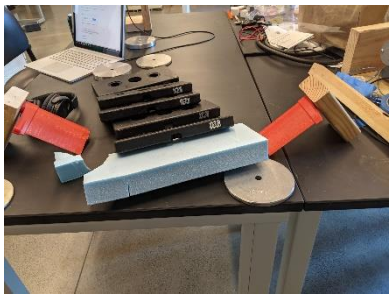

Figure 25: *Airfoil failure*

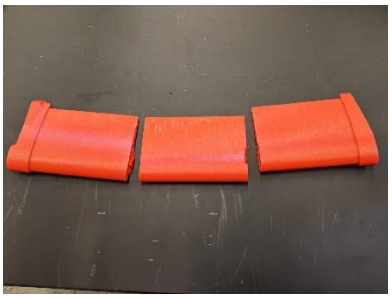

Figure 26: *Destroyed airfoil*

B. Wind Tunnel Testing

To test our turbine at CWC speeds, we modified our wind tunnel that we had built the previous year to

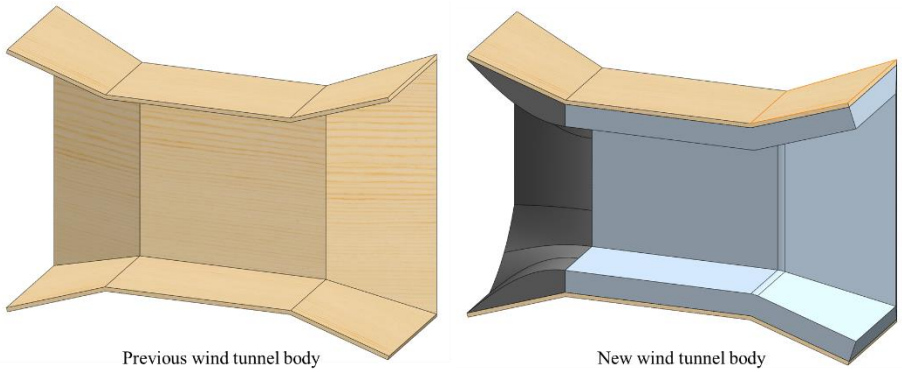

Figure 27: *Modifications to wind tunnel. In both images, the air flows to the left.*

create CWC wind conditions. The previous wind tunnel, shown in **Figure 27**, was a plywood construction with a fan on one end (not pictured). It was designed more for safety during a destructive test conducted last year than for good wind conditions. Because of this, it had poor flow conditions on the inside, producing

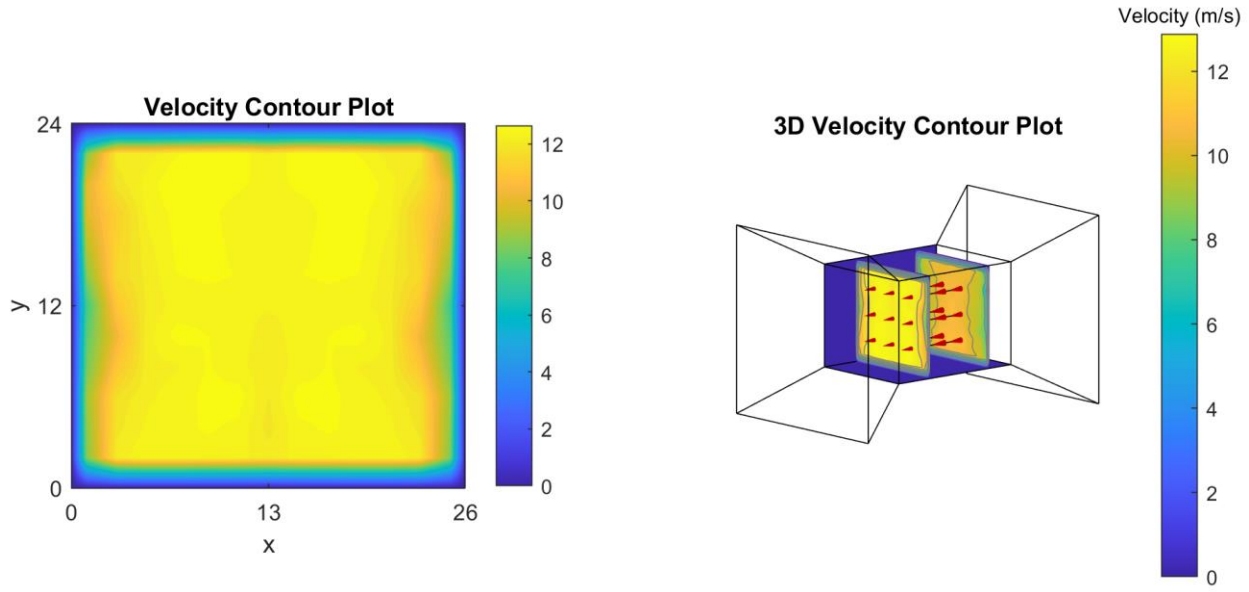

Figure 28: *Measured velocity contours inside the modified wind tunnel. 2D contour on the left was taken where we placed our turbine. In the 3D contour, the flow is to the left. Note that the velocity field is smoother farther downstream in the test section, which is where we placed our turbine.*

wind speeds of about 7 $\frac{m}{s}$ with a boundary layer 4 inches thick. To achieve both faster speeds and a better velocity profile, we lined the inside of the tunnel with 4 inches of foam and created smooth transitions over all the sharp edges. This raised the wind speed inside the tunnel to 12.3 $\frac{m}{s}$ and gave a much smoother profile. **Figure 28** shows the improved velocity profile inside the tunnel. The boundary layer was reduced to 2 inches, and excluding the boundary layer, the velocity was very consistent, with a standard deviation of 0.5 $\frac{m}{s}$ at the maximum wind speed.

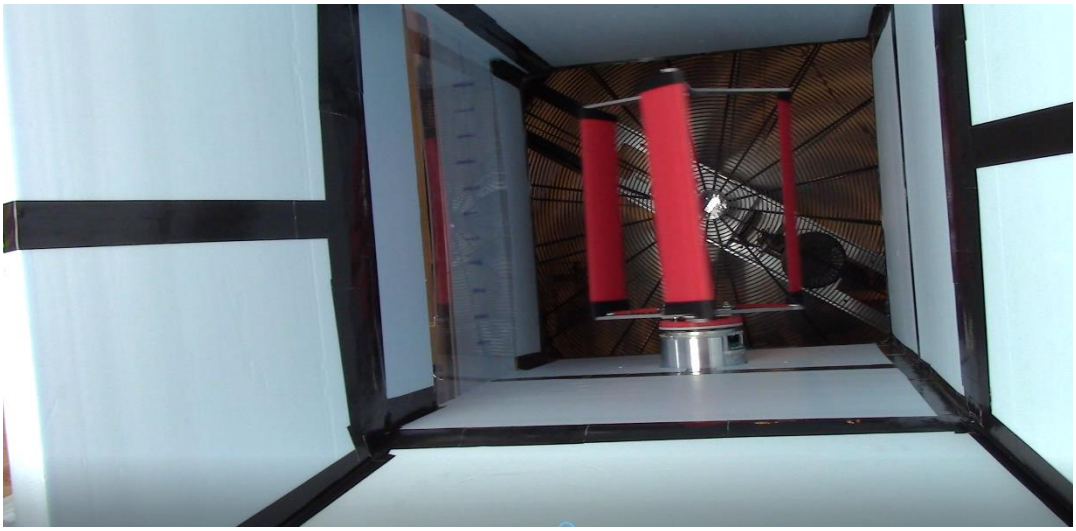

Figure 29: *Turbine mounted in wind tunnel*

In addition to reaching higher wind speeds, we also built a turntable to mount our turbine on, so we can spin it to test our yaw system. The turntable is rotated manually. **Figure 29** shows our assembled turbine in the wind tunnel. We plan to continue testing this turbine, but we were not able to work out some mechanical issues we had in time to try and collect power data from our turbine. Namely, we built our own gearbox this year, and it had a lot of resistance in it, which was enough to keep the turbine from spinning.

C. Commissioning Checklist

Due to the remote nature of the competition this year, the checklist provided will apply to the testing conditions in the wind tunnel used for the tests, rather than a full scale wind tunnel. Also because of space constraints in the test wind tunnel, the process may actually be more simple in full scale situations.

1. Separate turbine base in half, and thread base through hole in base of wind tunnel. Fasten back together, and bolt turbine to turntable mount beneath the wind tunnel.
2. Connect the three quick connect gold adapters from phase wires to rectifier
3. Connect wire bundle from control circuit to positions 1 (black/ground), 3 (orange/sensor), and 6 (red/hot) on the Hall Effect Sensor wire harness
4. Connect Yaw controls to stepper motor and wind direction sensor

VII. Conclusion

The Washington State University Everett Wind Energy team, in collaboration with Everett Community College Wind Energy team, designed a cycloturbine for CWC 2021, continuing our work from last year. Last year, while we were able to complete a lot of design work, ultimately, we were not able to build or test our prototype, leaving us uncertain of the functionality of many aspects of the design. This year, we began by reviewing our design and simplifying it so that we were able to build a full prototype. While we were not able to complete much testing of it, this prototype will serve as an excellent starting point for next year's team.

References

[1] Z. Adams and J. Chen, "Optimization and Validation of Cycloturbine Blade-Pitching Kinematics via Flux-Line Theory," *AIAA*, vol. 56, no. 5, pp. 1894-1909, 2018.

[2] D. Marten and J. Wendler, "QBlade Guidelines," 2013.

[3] Z. Adams and J. Chen, "Flux-Line Theory: A Novel Analytical Model for Cycloturbines," *AIAA*, vol. 55, no. 11, pp. 3851-3867, 11 2017.